Appl. Math. Mech. -Engl. Ed., **40**(7), 943–952 (2019)

Applied Mathematics and Mechanics (English Edition)

https://doi.org/10.1007/s10483-019-2495-8

Transient thermo-mechanical analysis for bimorph soft robot based on thermally responsive liquid crystal elastomers*

Yun CUI[1], Yafei YIN[1], Chengjun WANG[2], K. SIM[3],
Yuhang LI[1,4,†], Cunjiang YU[5,6,7,†], Jizhou SONG[2,†]

1. Institute of Solid Mechanics, Beihang University, Beijing 100191, China;
2. Department of Engineering Mechanics, Soft Matter Research Center,
Key Laboratory of Soft Machines and Smart Devices of Zhejiang Province,
Zhejiang University, Hangzhou 310027, China;
3. Materials Science and Engineering Program,
University of Houston, Houston, TX 77204, U. S. A.;
4. State Key Laboratory of Strength and Vibration of Mechanical Structures,
School of Aerospace Engineering, Xi'an Jiaotong University, Xi'an 710049, China;
5. Department of Mechanical Engineering, University of Houston, Houston, TX 77204, U. S. A.;
6. Department of Electrical and Computer Engineering, University of Houston,
Houston, TX 77204, U. S. A.;
7. Department of Biomedical Engineering, Texas Center for Superconductivity,
University of Houston, Houston, TX 77204, U. S. A.

(Received Dec. 9, 2018 / Revised Jan. 19, 2019)

Abstract Thermally responsive liquid crystal elastomers (LCEs) hold great promise in applications of soft robots and actuators because of the induced size and shape change with temperature. Experiments have successfully demonstrated that the LCE based bimorphs can be effective soft robots once integrated with soft sensors and thermal actuators. Here, we present an analytical transient thermo-mechanical model for a bimorph structure based soft robot, which consists of a strip of LCE and a thermal inert polymer actuated by an ultra-thin stretchable open-mesh shaped heater to mimic the unique locomotion behaviors of an inchworm. The coupled mechanical and thermal analysis based

* Citation: CUI, Y., YIN, Y. F., WANG, C. J., SIM, K., LI, Y. H., YU, C. J., and SONG, J. Z. Transient thermo-mechanical analysis for bimorph soft robot based on thermally responsive liquid crystal elastomers. *Applied Mathematics and Mechanics* (*English Edition*), **40**(7), 943–952 (2019) https://doi.org/10.1007/s10483-019-2495-8

† Corresponding authors, E-mail: liyuhang@buaa.edu.cn; cyu15@uh.edu; jzsong@zju.edu.cn

Project supported by the National Basic Research Program (No. 2015CB351901), the National Natural Science Foundation of China (Nos. 11372272, 11622221, 11621062, 11502009, and 11772030), the Doctoral New Investigator Grant from American Chemical Society Petroleum Research Fund of the National Science Foundation (Nos. 1509763 and 1554499), the Opening Fund of State Key Laboratory for Strength and Vibration of Mechanical Structures, Xi'an Jiaotong University (No. SV2018-KF-13), and the Fundamental Research Funds for the Central Universities (No. 2017XZZX002-11)

on the thermo-mechanical theory is carried out to underpin the transient bending behavior, and a systematic understanding is therefore achieved. The key analytical results reveal that the thickness and the modulus ratio of the LCE and the inert polymer layer dominate the transient bending deformation. The analytical results will not only render fundamental understanding of the actuation of bimorph structures, but also facilitate the rational design of soft robotics.

Key words transient thermo-mechanical analysis, soft robot, thermal-responsive, liquid crystal elastomer (LCE)

Chinese Library Classification O551, O302
2010 Mathematics Subject Classification 34B27, 74A15, 74S05

1 Introduction

Compared with traditional rigid robotics historically built for manufacturing product lines, soft robots, an emerging class of machines made from soft materials, offer unprecedented benefits of safety, adaptability, and complex motion[1–14]. Recent advances in materials and manufacturing technologies have boosted the fast development of soft robots. In particular, smart soft materials that change their shape and size upon being exposed to external stimuli offer a promising avenue to soft robots. Examples include dielectric elastomers (DEs)[3], electroactive polymers (EAPs)[4–6], shape memory alloys (SMAs)[7], shape memory polymers (SMPs)[6,8], hydrogels[9–10], and liquid crystal elastomers (LCEs)[11–13]. For instance, Wang et al.[11] developed an adaptive soft robot based on a thermal-responsive carbon black doped LCEs (LCE-CB) bimorph to mimic the locomotion behaviors of an inchworm. In addition, such an artificial soft robotic inchworm is able to sense the environmental change and to react to stimulation correspondingly. The thermal-responsive LCE-CB deforms with the change of its temperature due to phase transition[14–16]. As temperature is heated higher than the critical temperature of phase transition, the thermal-responsive LCEs shrink. The main components of the adaptive fully soft bodied robot[11] presented in Fig. 1(a) include actuators of ultra-thin stretchable heaters with the open-mesh shape[17–21] and thermally actuated artificial muscles based on a bimorph structure made up of LCE-CB and polyimide (PI, Kapton tape). The open-mesh shaped heater is electrically connected through an anisotropic conductive film (ACF) cable to supply power. Joule heat generates with the current injection into the ultra-thin deformable heater. The phase transition of the LCE-CB is then induced as the temperature increases, which causes shrinkage of the LCE-CB layer and thermal expansion of the PI layer in the bimorph structure, respectively. Since the thermal expansion of PI is pretty small ($\approx 0.01\%$) while the shrinking deformation of LCE-CB is relatively large ($\approx 24\%$) when the temperature reaches 100 °C after phase transition[11,22], a bending deformation of the bimorph structure shown in Fig. 1(b) will then be induced by the interface strain mismatch, which recovers its original shape after cooling.

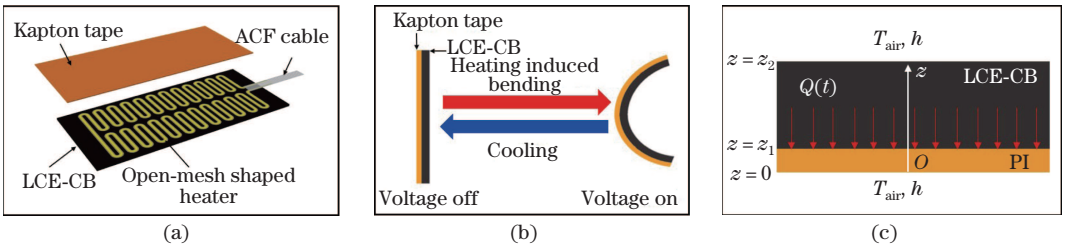

Fig. 1 (a) Illustration of the LCE-CB/PI bimorph structure with an ultra-thin stretchable heater at the interface, (b) thermal-induced bending deformation and cooling recovery of the bimorph structure, and (c) schematic diagram of the bimorph structure analytical model (color online)

The thermo-mechanical behavior of soft robots based on the LCE bimorph structure is important to their operation. Experimental characterization of the thermo-mechanical response time to reach the steady deformation is about 30 s[11]. To better understand the thermo-mechanical responses and to achieve improved designs for soft robots, an analytical model for describing the transient thermo-mechanical behavior is critically necessary to be established. To this end, this paper focuses on developing a transient thermo-mechanical analytical model to precisely capture both thermal and mechanical responses of the bimorph structure, which is further validated with the finite element analysis (FEA). The predictions of the temperature distribution and the curvature radius response induced by the heat generation from ultra-thin stretchable heaters are obtained from the model.

2 Mathematical modeling

Due to the two reasons as follows: (i) the thickness of the LCE-CB/PI bimorph structure (500 μm) larger than that of the stretchable heater composed of PI and gold (2.8 μm) by 2 orders of magnitude, and (ii) the significantly reduced bending stiffness from the open-mesh structure of the heater[11], it is rational to model the heater as a planar heat source which has few impacts on the bending of the bimorph structure. Considering that the stretchable heater's in-plane dimension (16.6 mm×7.9 mm) is almost the same as that of the bimorph structure (17.0 mm×9.4 mm)[11], the heat transfer of the structure can be approximately treated as a one-dimensional problem. As shown in Fig. 1(c), the soft robot[11] is then simplified as a bimorph structure with air convection boundary conditions on both sides (T_{air} and h denote the ambient temperature and the natural convection coefficient, respectively). The origin of the axis z along the thickness direction is located at the bottom surface of PI. The thickness of the PI layer is z_1 while the thickness of the LCE-CB layer is (z_2-z_1). Then, the Fourier heat conduction equations for this one-dimensional problem can be given as

$$\begin{cases} \dfrac{\partial \Delta T_1}{\partial t} - \alpha_1 \dfrac{\partial^2 \Delta T_1}{\partial z^2} = 0, \quad 0 \leqslant z < z_1, \\ \dfrac{\partial \Delta T_2}{\partial t} - \alpha_2 \dfrac{\partial^2 \Delta T_2}{\partial z^2} = \dfrac{\alpha_2}{k_2} Q(z,t), \quad z_1 \leqslant z \leqslant z_2, \end{cases} \tag{1}$$

where $\Delta T = T - T_{\text{air}}$ defines the temperature increase, which is the difference between temperature and T_{air}, and α and k are the thermal diffusivity and thermal conductivity of PI and LCE-CB with the subscripts 1 and 2, respectively. $Q(z,t) = Q_0 Q_1(z) Q_2(t)$ is the time-dependent planar heat source[23], where Q_0 is the amplitude of the input power, $Q_2(t)$ represents the time-variation of the unit power, while the δ function is used to describe $Q_1(z)$ as

$$Q_1(z) = \begin{cases} \infty, & z = z_1, \\ 0, & z \neq z_1, \end{cases}$$

where $\int_{z=z_1}^{z_2} Q_1(z) \mathrm{d}z = 1$.

The natural convection boundary conditions at both top ($z = z_2$) and bottom surfaces ($z = 0$) of the bimorph structure and the temperature/heat flux continuous conditions at the LCE-CB/PI interface ($z = z_1$) can be then given as follows:

$$\begin{cases} -k_1 \dfrac{\partial \Delta T_1}{\partial z} = -h \Delta T_1, \quad z = 0, \\ \Delta T_1 = \Delta T_2, \quad z = z_1, \\ k_1 \dfrac{\partial \Delta T_1}{\partial z} - k_2 \dfrac{\partial \Delta T_2}{\partial z} = 0, \quad z = z_1, \\ -k_2 \dfrac{\partial \Delta T_2}{\partial z} = h \Delta T_2, \quad z = z_2. \end{cases} \tag{2}$$

The initial conditions are

$$\begin{cases} \Delta T_1(z,0)=0, & 0\leqslant z<z_1, \\ \Delta T_2(z,0)=0, & z_1\leqslant z\leqslant z_2. \end{cases} \tag{3}$$

As a general and effective method, Green's function method[24] is used to solve Eq. (1). In order to obtain the appropriate Green's functions for the nonhomogeneous partial differential equations in Eq. (1), the homogeneous version of Eq. (1) is considered for the same region, which gives

$$\begin{cases} \dfrac{\partial\theta_1}{\partial t}-\alpha_1\dfrac{\partial^2\theta_1}{\partial z^2}=0, & 0\leqslant z<z_1, \\ \dfrac{\partial\theta_2}{\partial t}-\alpha_2\dfrac{\partial^2\theta_2}{\partial z^2}=0, & z_1\leqslant z\leqslant z_2, \end{cases} \tag{4}$$

and the corresponding boundary/initial conditions can be written as

$$\begin{cases} -k_1\dfrac{\partial\theta_1}{\partial z}=-h\theta_1, & z=0, \\ \theta_1=\theta_2, & z=z_1, \\ k_1\dfrac{\partial\theta_1}{\partial z}-k_2\dfrac{\partial\theta_2}{\partial z}=0, & z=z_1, \\ -k_2\dfrac{\partial\theta_2}{\partial z}=h\theta_2, & z=z_2, \end{cases} \tag{5}$$

$$\begin{cases} \theta_1(z,0)=0, & 0\leqslant z<z_1, \\ \theta_2(z,0)=0, & z_1\leqslant z\leqslant z_2. \end{cases} \tag{6}$$

Then, the method of separation of variables $\theta_i(z,t)=Z_i(z)\Gamma(t), i=1,2$ is used, and Eq. (4) turns to be

$$\frac{\partial\Gamma(t)}{\alpha_i\Gamma(t)\partial t}=\frac{\partial^2 Z_i(z)}{Z_i(t)\partial^2 z}=-\lambda_i^2 \tag{7}$$

with the following solutions:

$$\begin{cases} \Gamma(t)=\exp(-\alpha_i\lambda_i^2 t), \\ Z_1(\lambda_{1n},z)=A_{1n}\cos(\lambda_{1n}z)+B_{1n}\sin(\lambda_{1n}z), \\ Z_2(\lambda_{2n},z)=A_{2n}\cos(\lambda_{2n}z)+B_{2n}\sin(\lambda_{2n}z), \end{cases} \tag{8}$$

where

$$\begin{cases} A_{1n}=1, \\ B_{1n}=\dfrac{h}{k_1\lambda_{1n}}, \\ A_{2n}=\dfrac{\big(\cos(\lambda_{1n}z_1)+\frac{h}{k_1\lambda_{1n}}\sin(\lambda_{1n}z_1)\big)\big(\cos(\lambda_{2n}z_2)+\frac{h}{k_2\lambda_{2n}}\sin(\lambda_{2n}z_2)\big)}{\cos(\lambda_{2n}(z_2-z_1))+\frac{h}{k_2\lambda_{2n}}\sin(\lambda_{2n}(z_2-z_1))}, \\ B_{2n}=\dfrac{\big(\cos(\lambda_{1n}z_1)+\frac{h}{k_1\lambda_{1n}}\sin(\lambda_{1n}z_1)\big)\big(\sin(\lambda_{2n}z_2)-\frac{h}{k_2\lambda_{2n}}\cos(\lambda_{2n}z_2)\big)}{\cos(\lambda_{2n}(z_2-z_1))+\frac{h}{k_2\lambda_{2n}}\sin(\lambda_{2n}(z_2-z_1))}, \end{cases} \tag{9}$$

and the eigenvalues λ_{1n} and λ_{2n} satisfy

$$-hD_1(\lambda_{1n},\lambda_{2n})-k_1\lambda_{1n}D_2(\lambda_{1n},\lambda_{2n})=0 \tag{10}$$

with

$$D_1(\lambda_{1n},\lambda_{2n}) = \begin{vmatrix} \sin(\lambda_{1n}z_1) & -\cos(\lambda_{2n}z_1) & -\sin(\lambda_{2n}z_1) \\ k_1\lambda_{1n}\cos(\lambda_{1n}z_1) & k_2\lambda_{2n}\sin(\lambda_{2n}z_1) & -k_2\lambda_{2n}\cos(\lambda_{2n}z_1) \\ 0 & -k_2\lambda_{2n}\sin(\lambda_{2n}z_2)+h\cos(\lambda_{2n}z_2) & k_2\lambda_{2n}\cos(\lambda_{2n}z_2)+h\sin(\lambda_{2n}z_2) \end{vmatrix}, \tag{11a}$$

$$D_2(\lambda_{1n},\lambda_{2n}) = \begin{vmatrix} \cos(\lambda_{1n}z_1) & -\cos(\lambda_{2n}z_1) & -\sin(\lambda_{2n}z_1) \\ -k_1\lambda_{1n}\sin(\lambda_{1n}z_1) & k_2\lambda_{2n}\sin(\lambda_{2n}z_1) & -k_2\lambda_{2n}\cos(\lambda_{2n}z_1) \\ 0 & -k_2\lambda_{2n}\sin(\lambda_{2n}z_2)+h\cos(\lambda_{2n}z_2) & k_2\lambda_{2n}\cos(\lambda_{2n}z_2)+h\sin(\lambda_{2n}z_2) \end{vmatrix}. \tag{11b}$$

Combining the initial conditions given in Eq. (6), the complete solutions to Eq. (4) are obtained by the superposition principle as follows ($z_0 = 0$):

$$\theta_i(z,t) = \sum_{n=1}^{\infty} \frac{\Theta_n}{N_n} Z_i(\lambda_{in},z)\exp(-\alpha_i\lambda_{in}^2 t) \tag{12}$$

with $\Theta_n = \sum\limits_{r=1}^{2} \frac{k_r}{\alpha_r}\int_{z'=z_{r-1}}^{z_r} Z_r(\lambda_{rn},z')F_r(z')\mathrm{d}z'$ and $N_n = \sum\limits_{r=1}^{2} \frac{k_r}{\alpha_r}\int_{z'=z_{r-1}}^{z_r} Z_r^2(\lambda_{rn},z')\mathrm{d}z'$, which can be written in terms of Green's function as

$$\theta_i(z,t) = \sum_{j=1}^{2}\int_{z'=z_{j-1}}^{z_j} G_{ij}(z,t|z',\tau)|_{\tau=0}F_j(z')\mathrm{d}z', \tag{13}$$

and the forms of Green's functions of this problem are obtained by comparing the solutions in Eqs. (12) and (13) as

$$G_{ij}(z,t|z',\tau)|_{\tau=0} = \sum_{n=1}^{\infty} \frac{\exp(-\alpha_i\lambda_{in}^2 t)}{N_n}\frac{k_j}{\alpha_j} Z_j(\lambda_{jn},z')Z_i(\lambda_{in},z). \tag{14}$$

The desired Green's function can be derived by replacing t in Eq. (14) into $(t-\tau)$ as

$$G_{ij}(z,t|z',\tau) = \sum_{n=1}^{\infty} \frac{\exp(-\alpha_i\lambda_{in}^2 (t-\tau))}{N_n}\frac{k_j}{\alpha_j} Z_j(\lambda_{jn},z')Z_i(\lambda_{in},z). \tag{15}$$

Then, the solutions to Eq. (1) can be obtained according to Green's function method as

$$\begin{aligned} \Delta T_i(z,t) = \sum_{j=1}^{2}\Big(&\int_{z'=z_{j-1}}^{z_j} G_{ij}(z,t|z',\tau)|_{\tau=0}F_j(z')\mathrm{d}z' \\ &+ \int_{\tau=0}^{t}\mathrm{d}\tau\int_{z'=z_{j-1}}^{z_j} G_{ij}(z,t|z',\tau)\Big(\frac{\alpha_j}{k_j}g_j(z',\tau)\Big)\mathrm{d}z'\Big), \end{aligned} \tag{16}$$

where $z_0 = 0$, and $g_j(z',\tau)$ denotes the heat source term in the jth layer. Combining initial conditions and the heat source term together with Eq. (16), we can obtain

$$\Delta T_i(z,t) = \int_{\tau=0}^{t}\mathrm{d}\tau\int_{z'=z_1}^{z_2} G_{i2}(z,t|z',\tau)\Big(\frac{\alpha_2}{k_2}Q(z',\tau)\Big)\mathrm{d}z'. \tag{17}$$

Then, the analytical temperature predictions are presented by substituting Eq. (15) into Eq. (17) as follows:

$$\begin{cases} T_1(z,t) = T_{\mathrm{air}} + \sum\limits_{n=1}^{\infty}\dfrac{Q_0 Z_1(\lambda_{1n},z)}{N_n}G_n P_n(t), \\ T_2(z,t) = T_{\mathrm{air}} + \sum\limits_{n=1}^{\infty}\dfrac{Q_0 Z_2(\lambda_{2n},z)}{N_n}G_n P_n(t), \end{cases} \tag{18}$$

where

$$\begin{cases} G_n = \int_{z'=z_1}^{z_2} Z_2(\lambda_{2n}, z')Q_2(z')\mathrm{d}z', \\ P_n(t) = \int_{\tau=0}^{t} \exp(-\alpha_2\lambda_{2n}^2(t-\tau))Q_1(\tau)\mathrm{d}\tau. \end{cases} \tag{19}$$

As the temperature increases with time, the phase transition of LCEs will lead to the gradual shrinkage of the LCE-CB layer. At the same time, the thermal expansion of the PI layer will occur. Then, the bimorph structure will start to bend, i.e., induce the locomotion of the soft robot. Such kind of bending can be described by a bilayer beam model with initial strains in both layers[25], which are provided by thermal expansion of the PI layer and shrinking of the LCE-CB layer, respectively. Considering that the shrinking deformation of the LCE-CB layer ($\approx 24\%$) is much larger than the thermal expansion of the PI layer ($\approx 0.01\%$), the bending from mechanical mismatch is mainly attributed to the shrinkage of the LCE-CB layer[11]. Thus, only the initial thermal strain in the LCE-CB layer is taken into consideration in the following analysis. The bending normal stress σ_i of both layers can be obtained from Hooke's law,

$$\begin{cases} \sigma_1(z) = E_1\Big(c + \dfrac{z - z_\mathrm{b}}{R}\Big), \quad 0 \leqslant z < z_1, \\ \sigma_2(z) = E_2\Big(c + \dfrac{z - z_\mathrm{b}}{R} - \varepsilon_2^0(T_2)\Big), \quad z_1 \leqslant z \leqslant z_2, \end{cases} \tag{20}$$

where c denotes the uniform strain, z_b represents the neutral axis location, R is the bimorph structure' curvature radius, and E_i is Young's modulus of the ith layer. The shrinking strain $\varepsilon_2^0(T_2)$ in the LCE-CB layer can be obtained from the fitting functions[26] of the experimental data of shrinking strain's dependence on the temperature[11].

Since Young's modulus of the PI ($\approx 2\,\mathrm{GPa}$) is 4 orders of magnitude larger than that of LCE-CB ($\approx 0.5\,\mathrm{MPa}$), c is small enough to be negligible. An approximation based on the equilibrium of the bimorph structure can be given as follows:

$$\begin{cases} z_\mathrm{b} = \dfrac{E_1 z_1^2 + E_2(z_2^2 - z_1^2)}{2(E_1 z_1 + E_2(z_2 - z_1))}, \\ R \approx \dfrac{\int_0^{z_1} E_1(z - z_\mathrm{b})^2\mathrm{d}z + \int_{z_1}^{z_2} E_2(z - z_\mathrm{b})^2\mathrm{d}z}{\int_{z_1}^{z_2} E_2(z - z_\mathrm{b})\varepsilon_2^0(T_2)\mathrm{d}z}. \end{cases} \tag{21}$$

3 Results and discussion

The validation of the analytical results is carried out with the FEA based on the continuum element C3D8RT of the commercial software ABAQUS without any assumption. The stretchable heater is a PI/Au/PI sandwich structure with the thicknesses of 1.3 μm/200 nm/1.3 μm[11], respectively. The thicknesses of the PI and LCE-CB are 0.05 mm and 0.5 mm, respectively[11]. The thermal conductivity, thermal diffusivity, Young's modulus, and Poisson's ratio are, respectively, 317 $\mathrm{W{\cdot}m^{-1}{\cdot}K^{-1}}$, 1.54 $\times 10^{-6}\,\mathrm{m^2{\cdot}s^{-1}}$, 79 GPa, and 0.44 for gold[27]; 0.4 $\mathrm{W{\cdot}m^{-1}{\cdot}K^{-1}}$, $1.27\times 10^{-4}\,\mathrm{m^2{\cdot}s^{-1}}$, 0.5 MPa, and 0.5 for LCE-CB[11,28]; 0.12 $\mathrm{W{\cdot}m^{-1}{\cdot}K^{-1}}$, $7.75\times 10^{-8}\,\mathrm{m^2{\cdot}s^{-1}}$, 2.5 GPa, and 0.34 for PI[29]. The shrinking deformation dependence on the temperature of the LCE-CB from experiments is fitted with a piecewise linear function[26]. The thermal expansion coefficients for gold and PI are 15.4 $\times 10^{-6}\,\mathrm{K^{-1}}$ and $17.0\times 10^{-6}\,\mathrm{K^{-1}}$, respectively[26]. The natural convection coefficient is set as $h = 12\,\mathrm{W{\cdot}m^{-2}{\cdot}K^{-1}}$[26] while $T_\mathrm{air} = 25\,^\circ\mathrm{C}$, and the input power from heat source is 237 mW[11].

Figure 2(a) illustrates the condition of continuous constant heating input with $Q_2(t) = 1$. The maximum temperature in the bimorph structure occurs at the interface of the LCE-CB and

PI ($z = z_1$), and the time-variation of the maximum temperature derived from Eq. (18) is shown in Fig. 2(b), which agrees well with the FEA results. The maximum temperature increases from the initial ambient temperature of 25 °C to the steady-state temperature of 86.8 °C. It is shown that the temperature takes almost 30 s to reach the steady state, which indicates that the continuous constant heating source can affect the bending behavior for a relatively long time. The analytical predictions on the curvature radius from Eq. (21) are presented in Fig. 2(c). The results from the FEA agree well with the analytical predictions. The asymptote with the value of 3.921 mm represents the curvature radius under the steady-state temperature, which agrees well with the reported experimental result[11,26]. The curvature radius drops from 102.8 mm at 4 s to 4.7 mm after 20 s of heating. With the increase in the heating time, the changing trend of the curvature radius tends to be gentle, and the curvature radius gets closer and closer to the asymptote. Considering the situation that the motion of the soft robot needs to be controlled, a pulsed operation of the heater can be used to solve this problem. As shown in Fig. 2(d), the pulsed injected power can be modeled as

$$Q_2(t) = \begin{cases} 1, & kt_0 \leqslant t < kt_0 + t_\mathrm{p}, \\ 0, & kt_0 + t_\mathrm{p} \leqslant t \leqslant (k+1)t_0. \end{cases} \tag{22}$$

Then, the time-variation of the maximum temperature with the first three periods is presented in Fig. 2(e) with $t_0 = 25$ s and $t_\mathrm{p} = 25$ s. The temperature is almost stable after 3 periods as well as indicated by the curvature radius shown in Fig. 2(f). Through such a type of pulsed heating operation, the bending behavior of the soft robot can be controlled in a certain range (4.2 mm–27.4 mm) as shown in Fig. 2(f), instead of constant heating and complete cooling, which is an applicable method to control the soft robot.

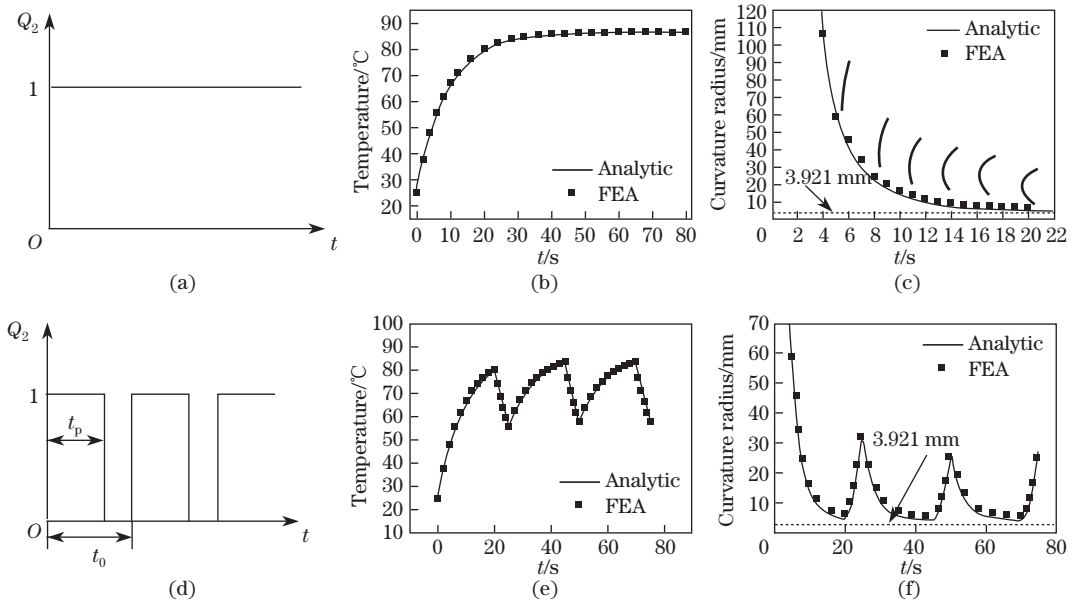

Fig. 2 (a) The constant unit power $Q_2(t)$, (b) the time-variation of the maximum temperature at the LCE-CB/PI interface under the constant injected power, (c) the time-variation of the bending curvature radius under the constant injected power, (d) the pulsed unit power $Q_2(t)$ with $t_\mathrm{p} = 20$ s and $t_0 = 25$ s, (e) the time-variation of the maximum temperature at the LCE-CB/PI interface under the pulsed injected power, and (f) the time-variation of the bending curvature radius under the pulsed injected power

Figure 3(a) presents the LCE-CB layer thickness influence on the bending curvature radius of the bimorph structure. As the LCE-CB thickness increases from 0.5 mm to 1.5 mm, the bimorph structure's bending curvature radius increases sharply at a certain time. Figure 3(b) shows the changing trend of the curvature radius versus the heating time under different modulus ratios E_1/E_2 of the bimorph structure. The results show that a larger modulus ratio will lead to a larger curvature radius at a certain time. These results indicate that, a thinner LCE-CB layer, the smaller modulus ratio E_1/E_2, and longer heating time before the steady state are helpful to generate a smaller curvature radius, i.e., significant movement of the soft robot.

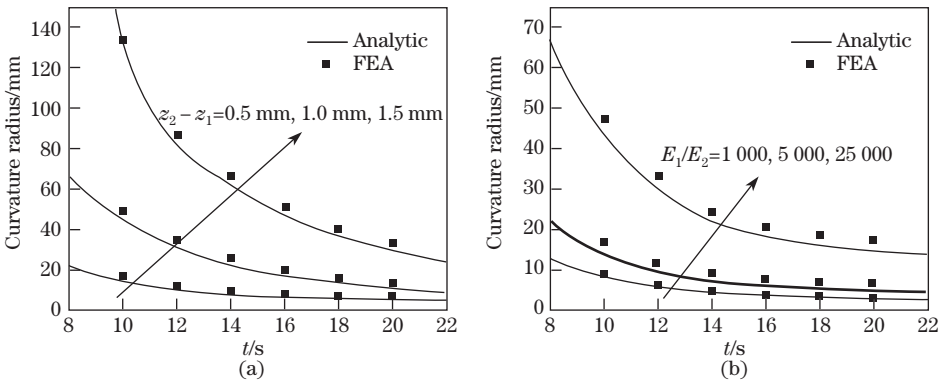

Fig. 3 (a) LCE-CB thickness influence on the bending curvature radius of the bimorph structure and (b) modulus ratio influence on the bending curvature radius of the bimorph structure

Another important parameter of concern is the response time, which is defined as the heating time when the curvature of the structure reaches 80% of the curvature at the steady state in this paper. The response time can be used to predict and design the motion period of the soft robot. The effects of the thicknesses of the LCE-CB and PI on the response time are shown in Figs. 4(a) and 4(b), respectively. The results suggest that a thicker structure will increase the response time under the same input power of 237 mW, which is acceptable. Since the bending of a thicker structure needs more energy, the response time will increase due to the constant input power. Figure 4(c) illustrates the influence of the input power on the response time. The response time tends to first increase and then decrease with the increase in the input power, which is mainly indicated by the strain-temperature curve of LCE-CB[11].

4 Conclusions

In summary, we have established a transient thermo-mechanical analytical model to predict the temperature field and locomotion of the LCE-CB bimorph based soft robot. This model precisely captures the thermal-induced bending process of the soft robot due to the Joule heating from the ultra-thin stretchable heater. Both analytical temperature and bending curvature predictions are in good agreement with those from the FEA. The key design parameters of the soft robot including the LCE-CB layer's thickness and the modulus ratio which affect the thermal response of the bimorph structure are systematically investigated. It is concluded that a thinner LCE-CB layer and a lower modulus ratio could yield more bending deformations. The response time and pulsed joule heat loading operation are also studied to shed light on the control and design of the soft robot. Overall, these results, from an analytical perspective, provide important insights and guidance for the design, fabrication, and control of the thermal responsive LCE based bimorph structured soft robots.

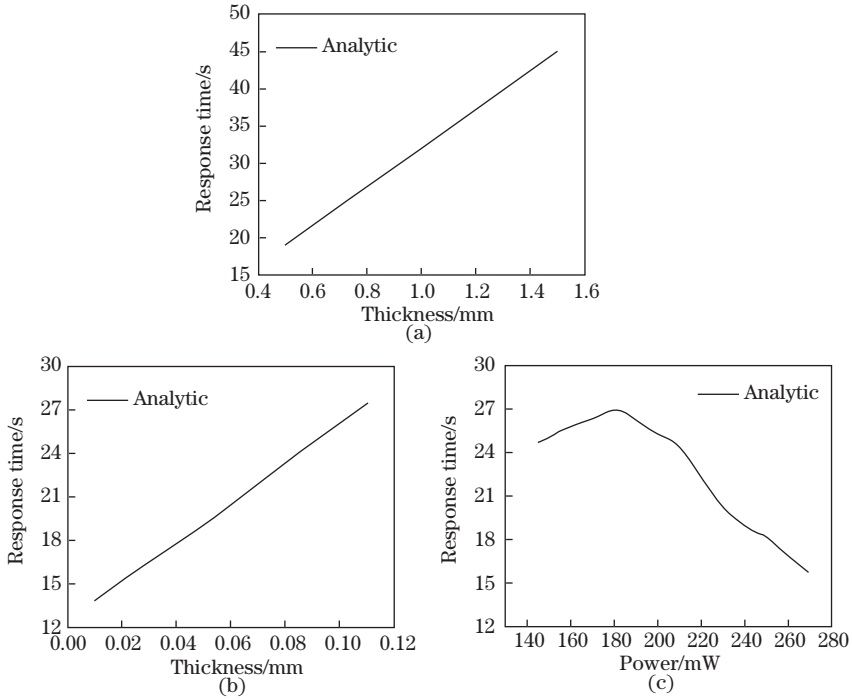

Fig. 4 (a) LCE-CB thickness influence on the bending response time of the bimorph structure, (b) PI thickness influence on the bending response time of the bimorph structure, and (c) injected power influence on the bending response time of the bimorph structure

References

[1] WEHNER, M., TRUBY, R. L., FITZGERALD, D. J., MOSADEGH, B., WHITESIDES, G. M., LEWIS, J. A., and WOOD, R. J. An integrated design and fabrication strategy for entirely soft, autonomous robots. *nature*, **536**(7617), 451–455 (2016)

[2] BARTLETT, N. W., TOLLEY, M. T., OVERVELDE, J. T. B., WEAVER, J. C., MOSADEGH, B., BERTOLDI, K., WHITESIDES, G. M., and WOOD, R. J. A 3D-printed, functionally graded soft robot powered by combustion. *Science*, **349**(6244), 161–165 (2015)

[3] GISBY, T. A., O'BRIEN, B. M., and ANDERSON, I. A. Self sensing feedback for dielectric elastomer actuators. *Applied Physics Letters*, **102**, 193703 (2013)

[4] LI, T. F., LI, G. R., LIANG, Y. M., CHENG, T. Y., DAI, J., YANG, X. X., LIU, B. Y., ZENG, Z. D., HUANG, Z. L., LUO, Y. W., XIE, T., and YANG, W. Fast-moving soft electronic fish. *Science Advances*, **3**, e1602045 (2017)

[5] KIM, D., KIM, K. J., TAK, Y., PUGAL, D., and PARK, I. Self-oscillating electroactive polymer actuator. *Applied Physics Letters*, **90**, 184104 (2007)

[6] REN, K. L., BORTOLIN, R. S., and ZHANG, Q. M. An investigation of a thermally steerable electroactive polymer/shape memory polymer hybrid actuator. *Applied Physics Letters*, **108**, 062901 (2016)

[7] LASCHI, C., CIANCHETTI, M., MAZZOLAI, B., MARGHERI, L., FOLLADOR, M., and DARIO, P. Soft robot arm inspired by the octopus. *Advanced Robotics*, **26**, 709–727 (2012)

[8] MENG, H. and LI, G. A review of stimuli-responsive shape memory polymer composites. *Polymer*, **54**(9), 2199–2221 (2013)

[9] PALLEAU, E., MORALES, D., DICKEY, M. D., and VELEY, O. D. Reversible patterning and actuation of hydrogels by electrically assisted ionoprinting. *Nature Communications*, **4**(4), 2257 (2013)

[10] MAEDA, S., KATO, T., KOGURE, H., and HOSOYA, N. Rapid response of thermo-sensitive hydrogels with porous structures. *Applied Physics Letters*, **106**, 171909 (2015)

[11] WANG, C. J., SIM, K., CHEN, J., KIM, H., RAO, Z., LI, Y. H., CHEN, W. Q., SONG, J. Z., VERDUZCO, R., and YU, C. J. Soft ultrathin electronics innervated adaptive fully soft robots. *Advanced Materials*, **30**, 1706695 (2018)

[12] LI, M. E., LV, S., and ZHOU, J. X. Photo-thermo-mechanically actuated bending and snapping kinetics of liquid crystal elastomer cantilever. *Smart Materials and Structures*, **23**, 125012 (2014)

[13] AN, N., LI, M. E., and ZHOU, J. X. Instability of liquid crystal elastomer. *Smart Materials and Structures*, **25**, 015016 (2016)

[14] YANG, T. Z., BAI, X., GAO, D. L., WU, L. Z., LI, B. W., THONG, J. T. L., and QIU, C. W. Invisible sensors: simultaneous sensing and camouflaging in multiphysical fields. *Advanced Materials*, **27**(47), 7752–7758 (2015)

[15] BEHL, M., KRATZ, K., NEOCHEL, U., SAUTER, T., and LENDLEIN, A. Temperature-memory polymer actuators. *Proceedings of the National Academy of Sciences of the United States of America*, **110**(31), 12555–12559 (2013)

[16] WHITE, T. J. and BROER, D. J. Programmable and adaptive mechanics with liquid crystal polymer networks and elastomers. *Nature Materials*, **14**(11), 1087–1098 (2015)

[17] HUANG, Y. A., DING, Y. J., BIAN, J., SU, Y. W., ZHOU, J., DUAN, Y. Q., and YIN, Z. P. Hyper-stretchable self-powered sensors based on electrohydrodynamically printed, self-similar piezoelectric nano/microfibers. *Nano Energy*, **40**, 432–439 (2017)

[18] ZHANG, Y. H., FU, H. R., SU, Y. W., XU, S., CHENG, H. Y., FAN, J. A., HWANG, K. C., ROGERS, J. A., and HUANG, Y. G. Mechanics of ultra-stretchable self-similar serpentine interconnects. *Acta Materialia*, **61**, 7816–7827 (2013)

[19] ZHANG, Y. H., HUANG, Y. G., and ROGERS, J. A. Mechanics of stretchable batteries and supercapacitors. *Current Opinion in Solid State and Materials Science*, **19**(3), 190–199 (2015)

[20] MA, Y. J., FENG, X., ROGERS, J. A., HUANG, Y. G., and ZHANG, Y. H. Design and application of 'J-shaped' stress-strain behavior in stretchable electronics: a review. *Lab on a Chip*, **17**(10), 1689–1704 (2017)

[21] CHEN, H., ZHU, F., JANG, K. I., FENG, X., ROGERS, J. A., ZHANG, Y. H., HUANG, Y. G., and MA, Y. J. The equivalent medium of cellular substrate under large stretching, with applications to stretchable electronics. *Journal of the Mechanics and Physics of Solids*, **120**, 199–207 (2018)

[22] LIU, Z. and GAO, J. Deformation-pattern-based digital speckle correlation for coefficient of thermal expansion evaluation of film. *Optics Express*, **19**, 17469–17479 (2011)

[23] SUN, Y. X., MA, J. X., LIU, S. B., and YANG, J. L. Analytical solution of transient heat conduction in a bi-layered circular plate irradiated by laser pulse. *Canadian Journal of Physics*, **95**(4), 322–330 (2017)

[24] CHEN, T. M. and CHEN, C. C. Numerical solution for the hyperbolic heat conduction problems in the radial-spherical coordinate system using a hybrid Green's function method. *International Journal of Thermal Sciences*, **49**(7), 1193–1196 (2010)

[25] NILISHKOV, J. P. Curvature estimation for multilayer hinged structures with initial strains. *Journal of Applied Physics*, **94**(8), 5333–5336 (2003)

[26] CUI, Y., WANG, C. J., SIM, K., CHEN, J., LI, Y. H., XING, Y. F., YU, C. J., and SONG, J. Z. A simple analytical thermo-mechanical model for liquid crystal elastomer bilayer structures. *AIP Advances*, **8**, 025215 (2018)

[27] YU, C. J., DUAN, Z., YUAN, P. X., LI, Y. H., SU, Y. W., ZHANG, X., PAN, Y. P., DAI, L. L., NUZZO, R. G., HUANG, Y. G., JIANG, H. Q., and ROGERS, J. A. Electronically programmable, reversible shape change in two- and three-dimensional hydrogel structures. *Advanced Materials*, **25**(11), 1541–1546 (2013)

[28] TORRAS, N., ZINOVIEV, K. E., CAMARGO, C. J., CAMPO, E. M., CAMPANELLA, H., ESTEVE, J., MARSGALL, J. E., TERENTJEV, E. M., OMASTOVA, M., and KRUPA, I. Tactile device based on opto-mechanical actuation of liquid crystal elastomers. *Sensors and Actuators A: Physical*, **208**, 104–112 (2014)

[29] DuPont. Kapton® HN general-purpose polyimide film (2018) https://www.dupont.com/products/kapton-hn.html